Emergence of tipping points and transient dynamics in finite observations

Sergio Cobo-López[1,2,3], Lucas J. Carbajal[4], Matthew Witt[1,5,6], Forest L. Rohwer[1,2], and Antoni Luque[1,4,7,*]

[1]Viral Information Institute, San Diego State University, San Diego, CA 92182, USA.
[2]Department of Biology, San Diego State University, San Diego, CA 92182, USA.
[3]Department d'Enginyeria Química, Universitat Rovira i Virgili, Tarragona, Catalonia, Spain.
[4]Department of Biology, University of Miami, Miami, FL 33146, USA.
[5]Department of Physics, San Diego State University, San Diego, CA 92182, USA.
[6]Holland Artificial Intelligence, San Diego, CA, USA.
[7]Department of Physics, University of Miami, Miami, FL 33146, USA.
[*]Corresponding author: antoni.luque@miami.edu

ABSTRACT

The dynamics of biogeochemical, ecological, and astronomical systems are transient. Yet, predicting the occurrence of dynamical shifts remains a challenge due to inferential uncertainties from datasets and the limitations of asymptotic-dependent theories. To address this problem, we developed a theoretical framework that builds on the finite nature of observations. This framework assesses the relative importance of processes, defined as the mechanisms that contribute to the rate of change of the system's dynamic variables, and it predicts the critical values that would trigger a shift into a new regime. The number of observable dynamic regimes within the framework increases exponentially with the number of processes. Observers, however, only experience dynamic regimes associated with relevant processes—those exceeding a tipping point—within their reference framework. A case study of the framework was tested for a classic predator-prey system with four processes parameterized for bacteria (prey) and lytic bacteriophages (predator). The analysis recovered the sixteen dynamic regimes predicted by the framework, including two non-trivial quasi-equilibrium dynamics. An adaptive Boolean model, which used only relevant observable processes, validated the accuracy of the framework, recovering the dynamics of the full model. The observational framework introduced here provides a strategy for identifying the processes and conditions that lead to tipping points, representing a conceptual paradigm

shift in transient dynamics, placing the focus on the specific, finite context of the observer, rather than the intrinsic, asymptotic states of the system.

SIGNIFICANCE

Sudden shifts in ecological, climate, and biological systems—so-called tipping points or critical transitions—are notoriously difficult to predict. This study introduces a mathematical framework that redefines these transitions as outcomes shaped by the observer's empirical limits. By accounting for finite observation time and resolution, the framework uncovers a rich spectrum of dynamic regimes that classical theories overlook. Its conceptual rigor and practical value are demonstrated in a predator-prey system. This new approach reframes how to forecast regime shifts in complex systems and offers a tool with broad relevance, from microbial ecosystems to planetary climate.

KEYWORDS

Transient dynamics, tipping points, Boolean dynamics, predator-prey systems, bacteriophages.

INTRODUCTION

Natural systems are transient. The emergence of marine photosynthetic bacteria triggered a transition from low to high oxygen in the atmosphere 2.5 billion years ago (Lyons et al., 2014; Margulis & Sagan, 1997). The disruption of the thermohaline circulation in the Atlantic during the Younger-Dryas period reversed the recovery from the last Glaciation period 12,000 years ago (Cheng et al., 2020; Scheffer, 2009). The increase in overfishing and eutrophication is favoring fleshy algae to outcompete calcifying corals and coralline algae, transforming the trophic structure in coral reefs towards a microbialized ecosystem (Haas et al., 2016; Pogoreutz et al., 2017; Silveira et al., 2019). These are just a few examples of the prevalence of transient dynamics in ecological, climate, and social systems (Gladwell, 2000;

Hastings et al., 2018; Scheffer, 2009; D. Seekell, 2016). However, predicting such major transitions and their consequences remains a pressing challenge.

A promising strategy for predicting transitions in natural systems is the use of early warning signals, based on statistical patterns in dynamic variables, as a proxy for an upcoming transition (Bury et al., 2021; Clements et al., 2019; Dakos et al., 2024; Scheffer et al., 2009). The majority of these methods are data-driven and use statistical and machine learning approaches to exploit or identify signals that can be informative, such as mean rates, conditional heteroskedasticity, or deep-learning-based patterns (Bury et al., 2021; Ditlevsen & Ditlevsen, 2023; Oro et al., 2023; Pedersen et al., 2020; Rocha et al., 2018; D. A. Seekell et al., 2011). However, these early warning indicators strongly depend on the dataset used, leading to issues with reliability and uncertainty quantification (Boettiger & Hastings, 2012). Using physical-based frameworks grounded in critical transition theory offers a more generalizable approach as a guide for early warning signals (Scheffer et al., 2009). This assumption is based on the idea that transitions depend on asymptotic attractors between equilibrium states (Hastings et al., 2018). However, empirical tests have demonstrated that the assumptions underlying the application of critical transition theory do not always hold for natural systems (O'Brien et al., 2023).

A significant limitation of current theoretical frameworks that study transient dynamics is their reliance on concepts rooted in asymptotic dynamics and equilibrium states (Hastings et al., 2018; Scheffer, 2009). The influence of ideas and methods associated with asymptotic time comes from the fact that these are well-established and fruitful approaches in the mathematical theory of dynamical systems and their application in theoretical physics and mathematical biology (Murray, 2007; Strogatz, 2015). The fact that these asymptotic methods can obtain elegant theoretical results describing transitions when fast processes and slow processes co-occur represents a persuasive argument for their use in characterizing transient dynamics (Kevorkian & Cole, 1981; Strogatz, 2015). However, most studies that use mechanistic models to investigate the underlying processes causing transitions in dynamical systems rely on ad-hoc analyses of the dynamic trajectories on the regions of interest (Bashkirtseva & Ryashko, 2018; Cairns et al., 2009; Cushing et al., 1998; Rabinovich et al., 2006; Rinaldi & Scheffer, 2000; Roach et al.,

2017). This leads to interpretations that depend strongly on the specific numerical values used in the dynamics, but are difficult to generalize, limiting the ability to predict the parameter values or conditions that can generate unexpected transitions. Sophisticated approaches that can extract transient dynamics regimes, like Lyapunov exponents, sloppy model theory, and low-dimensional manifolds, are not trivial to implement and do not necessarily lead to theoretical expressions revealing the underpinning causes of the transitions (Gutenkunst et al., 2007; Jiang et al., 2018; Mao et al., 2024; Ponce-Alvarez et al., 2020; Wadduwage et al., 2013; Wolf et al., 1985). Both the data-driven and the asymptotic-based mechanistic methods, thus, are currently limited in their ability to generalize the insights obtained from studying transitions in specific systems, posing a challenge in predicting the conditions that could lead to future transitions in natural systems.

An underlying premise across current methodologies investigating transient dynamics is the assumption that transient regimes and their associated critical values or tipping points are an intrinsic property that is somehow inherent to the system and awaits to be characterized or inferred (Gladwell, 2000; Hastings et al., 2018; Scheffer, 2009; D. Seekell, 2016). A factor that is overlooked, however, is the fact that it is the observer who ultimately distinguishes, based on measurements, perception, and prior knowledge, what is interpreted as a significant change in the dynamics of a system (Kuhn, 2012; Swain et al., 2021; Zimring, 2019). The temperature during a conference may be considered constant by the audience as long as it remains within a certain degree Celsius range, regardless of fluctuations below that threshold (Battistel et al., 2023; Yuasa et al., 2024; Zhou et al., 2022). However, a one-degree change in laboratory conditions can result in a significant change in chemical reactions (McLeod et al., 2025; Petersen et al., 2023). The temperature oscillations would be discarded as noise in the first case, but characterized carefully and controlled, if possible, in the second case. It is the observer who, based on their own goals, context, and technology, interprets the same data as either constant or transient. This requires developing methods to investigate transient dynamics, building on the constraints associated with the observer instead of the asymptotic properties or general intrinsic signals of a system. This article aims to fill this key fundamental gap in transient dynamics.

The framework introduced here builds on two empirical principles (Figure 1). First, any observer interacts with, measures, or aims to predict the behavior of a system for a finite amount of time, which defines the observational time. Second, any observer has a finite perception of the change in a dynamic variable or agent, limited by their capability or context. Only changes above this finite threshold are perceptible or of interest in the context. The ratio of these two finite magnitudes determines the relevant observable rate for an observer (Figure 1). The contribution of each dynamic process relative to the observable rate determines the weight of the process perceived by the observer (Figure 1). Only processes above the observable rate are considered relevant for the observer. The dynamic conditions leading to a process to cross the observable rate are associated with critical values or tipping points and define the observable dynamic regimes. Here, this general framework was applied to a classic predator-prey system as a proof of concept. The predicted dynamic regimes were examined in the context of bacteria (prey) and bacteriophages (predators). The theoretical framework predicted transient regimes that had been previously overlooked, and the predictions were tested by measuring the error between the full dynamical system and the system including only the observable processes. The addition of a new process, associated with the population's carrying capacity, was used to test the framework's ability to predict the conditions under which such a process would be observable. The discussion section elaborates on how the insight gained from the finite observable framework offers a guide to diagnosing and predicting transient dynamics.

METHODS

Identification of dynamic regimes and tipping points in the observational reference framework. The observational framework was defined based on the relevant observational time Δt_{obs} and relevant observational change $\Delta A_{i,obs}$ for each agent (or observable dynamic variable) A_i. Their ratio defined the relevant observable rate $W_{i,obs} = \frac{\Delta A_{i,obs}}{\Delta t_{obs}}$. The dynamics of each agent A_i was defined as the net rate of

change, summing the processes F_{ij}. Normalizing the rates using the relevant observable rate yielded the weight of each process $w_{ij} = \frac{F_{ij}}{W_{i,obs}}$. A process was considered dynamically relevant if its rate exceeded the observable rate, which in terms of weights led to the condition $w > w_{th} = 1$, with w_{th} being the observable threshold (tipping point). The values of the dynamic variables at the tipping point were defined as the critical values, $A_{i,c}$,. Each dynamic regime was defined as a unique set of relevant processes. The key steps in this process are illustrated in Figure 1.

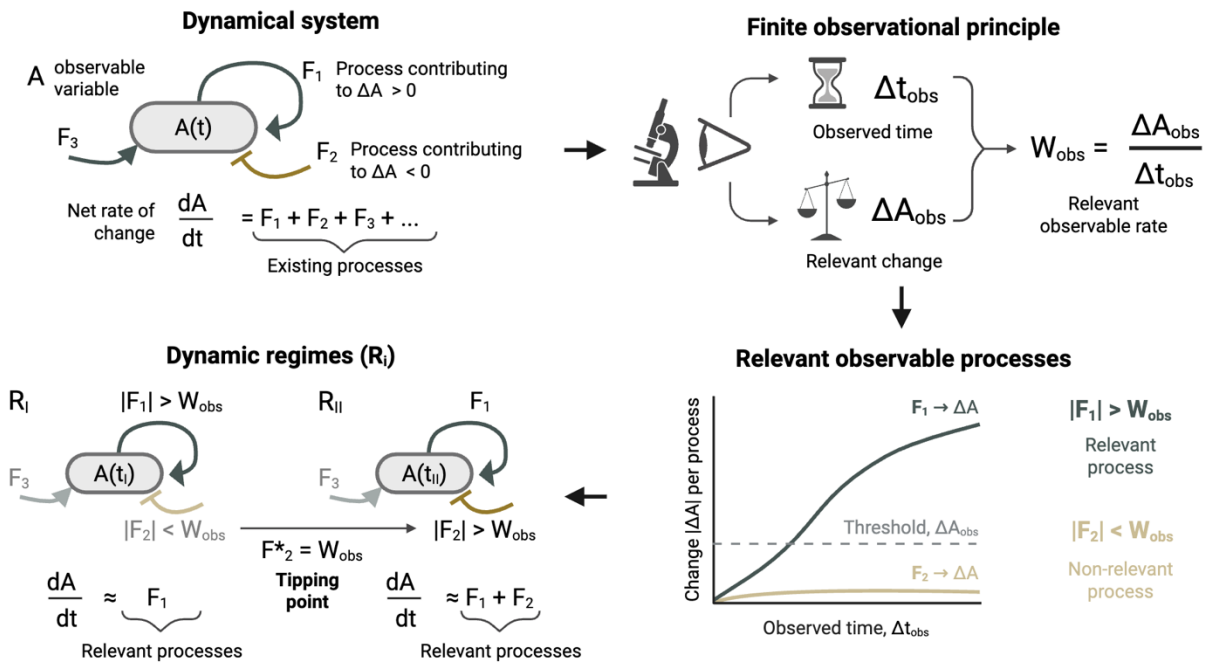

Figure 1. Dynamic regimes in the finite observational framework. The description below follows the same order as the arrows connecting the panels. (Top left) Diagram of a dynamical system illustrating the impact of different processes, F_i, on the observable dynamic agent or variable, A(t). A few processes contributing to a positive change ΔA>0 (dark blue arrow) or negative change ΔA<0 (gold flat-head arrow) are illustrated. The equation at the bottom displays the contribution of the processes to the net rate of change, dA/dt. (Top right) Diagram illustrating the two finite observational principles: the finite observed time, Δt^{obs}, and the relevant perceived change, ΔA^{obs}. Their ratio leads to the relevant observable rate, W^{obs}. (Bottom right) Graph illustrating the individual contribution of two processes to the change of A over the observed time. The dashed horizontal grey line indicates the threshold associated with the relevant perceived change ΔA^{obs}. Processes above this threshold are displayed as relevant (opaque) and below as non-relevant (semi-transparent). Their relationship with the relevant observable rate, W^{obs} is displayed. (Bottom left) Diagram displaying a transition between dynamics regimes R_I and R_{II}, characterized each by different relevant processes. The condition for the tipping point responsible for the transition is displayed as F^*_i. Figure created in BioRender as open access https://BioRender.com/5g3o22z.

Dynamic regimes and tipping points in a Lotka-Volterra system for phage and bacteria. The bacteria (prey), $A_1 = B$, and a lytic bacteriophage (predator), $A_2 = P$, dynamics were approximated using a standard Lotka-Volterra model (Weitz, 2016). The net rate of change of the bacterial population was defined by two processes: the bacteria growth rate, $F_{11} = F_g$, and the phage infection or predation pressure, $F_{12} = F_p$ (see differential equations in Figure 2a). The net rate of change of the phage population was also defined by two processes: the phage production or burst when lysing an infected cell, $F_{21} = F_b$, and the phage decay rate, $F_{22} = F_d$ (Figure 2a). The observational time was defined as $\tau = \Delta t_{obs}$, while the relevant observational change of phage and bacteria was set, respectively, to $\Delta B_{obs} = \alpha \cdot B$ and $\Delta P_{obs} = \alpha \cdot P$. Here α was the fraction of the population change considered to be relevant in the observation. The weights of each process and the critical concentrations associated with tipping points were obtained by following the prescriptions described in the previous section and are presented in the Results. The dynamic regimes were defined by different combinations of relevant processes for the observer.

*Attractors of the dynamic regimes***.** The theoretical attractors were derived as the asymptotic solution, that is, for infinite observational time, for each subset of differential equations within each dynamic regime. If a fixed point existed (making the rates of the system equal to zero), then the linear stability of the fixed point was evaluated by the eigenvalues of the Jacobian, following standard practices (Strogatz, 2015). The analysis is available in the Supplementary Information (S1. Asymptotic Analysis).

Model parametrization. The range of values for the agents, parameters, and typical observational times in the model was obtained from the literature for both laboratory experiments and environmental studies, as summarized in Table 1 and expanded in the Supplementary Information (S2. Model Parametrization). In the numerical analysis, the observer's tolerance (or relevance threshold) was set to $\alpha = 0.1$, that is, a 10% change in the population.

Numerical simulations. Case studies illustrating all predicted dynamic regimes in the observational framework were explored following the theoretical analysis shared in the Results section. This resulted in four sets of parameter values (one for each scenario), which were selected based on a

rationale that incorporated laboratory and environmental values (Table 1). For scenarios predicted to produce quasi-equilibrium solutions, two sets of initial conditions were used, capturing both quasi-equilibrium and transient trajectories. The system of differential equations was coded in Python and integrated with the *solve_ivp* function in *scipy* library (Virtanen et al., 2020). This function relies on the LSODA solver from the FORTRAN library odepack (Hindmarsh, 1983), which automatically switches between non-stiff and stiff solvers depending on the behavior of the equations (Petzold, 1983). The code developed to generate the simulations is available on GitHub (https://github.com/luquelab/transient-dynamics). The simulated dynamics, including populations, weights, and relevant processes, are provided in the Supplementary Information (S3. Simulated Dynamics).

Table 1. Model parametrization. The columns display the values for the model parameters, bacteria and phage concentrations, and observational (obser.) time. The units are in parentheses. The rows distinguish the empirical ranges and the values used in each dynamic scenario. For each scenario, the concentrations of phage and bacteria correspond to the initial conditions used. (*) For the agents' concentrations, the scenarios correspond to the initial values; scenarios with two lines of initial values correspond to the transient dynamics case (tr.) and the quasi-equilibrium case (q.-eq.). The Supplementary Information (S2. Model Parametrization) includes how different references contributed to build these ranges (Anthenelli et al., 2020; Brum et al., 2016; K. Cheng et al., 2007; De Paepe & Taddei, 2006; Kannoly et al., 2023; Luque & Silveira, 2020; Silveira et al., 2021; Suttle & Chen, 1992)

	Growth rate, r (h)	Infection rate, a (ml·h^{-1})	Burst size, c (phages)	Decay rate, m (h^{-1})	*Bacteria concentration, B (cells·ml^{-1})	*Phage concentration P (phages·ml^{-1})	Obser. time, τ (h)
Ranges	$3\cdot10^{-5}$–6	$7\cdot10^{-10}$–$1\cdot10^{-6}$	2–5,000	10^{-3}–0.8	$1\cdot10^{-4}$–$8\cdot10^{9}$	$1\cdot10^{-4}$–$2\cdot10^{10}$	0.8 – 16,800
Scenario 1	Based on laboratory values associated with fast growing bacteria (*E. coli*-like) and lytic phage (T4-like)						
	0.9	$3\cdot10^{-8}$	50	$1.5\cdot10^{-3}$	10^{3}	10^{4}	14
Scenario 2	Based on environmental marine communities of slow growing bacteria and fast decaying phage (UV-exposed)						
	$3.2\cdot10^{-5}$	$1\cdot10^{-10}$	225	$1\cdot10^{-1}$	$6.7\cdot10^{7}$	$1\cdot10^{0}$	260
Scenario 3	Based on environmental communities (coastal-like) of relatively fast-growing bacteria and fast decaying phage						
	$1\cdot10^{-1}$	$3\cdot10^{-9}$	50	$1\cdot10^{-1}$	$2.65\cdot10^{3}$ (tr.) $6\cdot10^{5}$ (q-eq)	$4.93\cdot10^{4}$ (tr.) $6\cdot10^{6}$ (q-eq)	300
Scenario 4	Based on deep ocean-like communities of slow growing bacteria and slow decaying phage						
	$3.2\cdot10^{-5}$	$3\cdot10^{-8}$	50	$1.5\cdot10^{-3}$	$8.5\cdot10^{5}$ (tr.) $1\cdot10^{3}$ (q.-eq)	$3\cdot10^{3}$ (tr.) $1\cdot10^{4}$ (q.-eq)	13

Error analysis of the predicted regimes. To test the accuracy of the observational framework, the full phage-bacteria model (Figure 2a) was compared with a dynamically adaptive Boolean model that integrated only the relevant processes in a regime (Shmulevich & Kauffman, 2004; Wang et al., 2012).

The adaptive differential equation model was obtained by multiplying each process of the original model by a Heaviside step function $\theta_i(w_i - w_{th}))$ = 1 for $w_i \geq w_{th}$ and 0 otherwise, where w_i was the weight of process *i* and w_{th} = 1 was the threshold. This differential equation was integrated for the same initial conditions, parameters, and methods as the full model. The error for each population was obtained as the absolute difference between the value from the full and adaptive models at each time step. The relative error was defined as the absolute error divided by the value of the full model. The combined error was defined as the average of the relative errors of the populations at each time step. Summary statistics were obtained for each regime, scenario, and overall simulation dynamics.

Analyzing the impact of adding a new process. The phage-bacteria model, defined by the Lotka-Volterra equations, was modified by incorporating a carrying capacity process as described in the Results section. This process accounted for the competition between bacteria for resources (Murray, 2007; Weitz, 2016). The weight of the carrying capacity process w_K was obtained using the observational framework. Conditions associated with the quasi-equilibrium solution of the standard model were used to assess the impact of the process on the system (Table 1). The observational framework was used to predict the critical observational time needed to observe the effect of the carrying capacity process ($w_K > w_{th} = 1$). The full and adaptive models were simulated and compared to assess the errors of the observational framework.

RESULTS

General predictions derived from the finite observational reference framework.

Tipping points depend on the observer. The normalization of the j-th process, F_{ij}, in the dynamics of the observable variable or agent A_i with respect to the reference observational rate, $W_i^{obs} = \frac{\Delta A_i^{obs}}{\Delta t^{obs}}$, determined

the weight of each process $w_{ij} = \frac{F_{ij}}{r_i^{obs}}$ in the observer's reference framework (Figure 1). Here, Δt^{obs} was the relevant observational time and ΔA_i^{obs} the relevant observational change for agent i. A process was predicted to be relevant if its rate was similar to or larger than the observational rate $|F_{ij}| \geq W_i^{obs}$, leading to the weight-based condition for relevance:

A process, F_{ij}, is relevant if its weight, $w_{ij} = \frac{F_{ij}}{W_i^{obs}}$, satisfies $|w_{ij}| \geq w_{th} = 1$. Eq. (1)

Here, w_{th} was the critical threshold. The critical values of the variables and parameters leading to the threshold value $|w_{ij}^*| = w_{th} = 1$ or tipping point were predicted to determine when a process switches from relevant to irrelevant or vice versa (Figure 1). Two observers subject to different observational rates, $W_i^{obs(1)} \neq W_i^{obs(2)}$either through the observational time or a relevant observational change will perceive different weights for the same process, $w_{ij}^{obs(1)} \neq w_{ij}^{obs(2)}$, or, equivalently, tipping points at different critical values. An asymptotic observational time, $\Delta t^{obs} \to \infty$, or infinitely precise observational change, $\Delta A^{obs} \to 0$, led to weights that were infinite, $w_{ij} \to \infty$, making the associated process always relevant, and no tipping points would exist. Therefore, tipping points associated with a dynamic process are an emerging property of the observer's finite observational reference framework.

The dynamic regimes increase exponentially with the number of processes. The relevant processes impacting the dynamics can lead variables to cross critical values, making other previously irrelevant processes relevant or vice versa (Figure 1). Each process in a dynamical system can be either relevant or irrelevant, and, thus, the number of dynamic regimes, *D*, that an observer can perceive is predicted to grow exponentially with the number of processes, M, in the system:

In a system with $M = \sum_{i=1}^{N} n_i$ processes there are $D \leq 2^M$ observable dynamic regimes. Eq. (2)

Systems with more processes, thus, can lead to exponentially more complex observable dynamics. Suppose a system remains in the same dynamic regime during the observational time. In that case, the asymptotic attractors during the observation will stay the same, leading the observer to perceive the

247 dynamics as more predictable or *quasi-steady*. Suppose the dynamics stay in the same regime and the
248 variables oscillate around or converge towards a constant value. In that case, the observer may interpret
249 the system as being in a *quasi-equilibrium state*. In the limit case, where the value of dynamic variables
250 remains within the relevant observable change, the observer may perceive the system as *quasi-static*.
251

252 **The case study of a classic predator-prey system in the context of phage and bacteria confirmed the**
253 **general predictions.**

254 ***Sixteen dynamic regimes were observed, distributed in four scenarios.*** The normalization of the phage
255 and bacteria (Lotka-Volterra) model (Figure 2a) using the observational framework yielded the equation
256 rates in terms of the weights, w, for the four processes ($M = 4$) in the system, that is, bacterial growth (w_g)
257 and phage predation (w_p) for the bacterial rate of change, and the phage production or burst (w_p) and
258 phage decay (w_d) for the phage rate of change:

$$\frac{\tau}{\alpha B}\frac{dB}{dt} = \underbrace{\frac{\tau\, r}{\alpha}}_{growth,\, w_g} - \underbrace{\frac{\tau\, a\, P}{\alpha}}_{predation,\, w_p} \qquad \text{Eq. (3)}$$

$$\frac{\tau}{\alpha B}\frac{dB}{dt} = \underbrace{\frac{\tau\, c\, a\, B}{\alpha}}_{burst,\, w_b} - \underbrace{\frac{\tau\, m}{\alpha}}_{decay,\, w_d}$$

259 Here, r was the bacterial intrinsic growth rate constant, a the adsorption-infection rate constant, c the
260 phage burst size, and m the phage decay rate constant. The parameter α was the observational tolerance
261 used in the relevant observational changes $\Delta B^{obs} = \alpha B$ and $\Delta P^{obs} = \alpha P$. This led to constant weights
262 for the growth rate, w_g, and phage decay, w_d, Eq. (3). These processes were predicted to be observable
263 ($w > w_{th} = 1$) for observational times $\tau \geq \tau_g = \alpha/r$ and $\tau \geq \tau_d = \alpha/m$, respectively. The weights for the
264 predation, w_p, and phage burst (or production), w_b, depended dynamically on the phage population, P,
265 and the bacterial population, B, respectively, Eq. (3). Thus, the threshold (or tipping point), $w_{th} = 1$,
266 predicted the critical concentrations $P_c = \alpha/(\tau\, a)$, and $B_c = \alpha/(\tau\, c\, a)$ for the predation and phage burst
267 to become relevant processes, respectively.

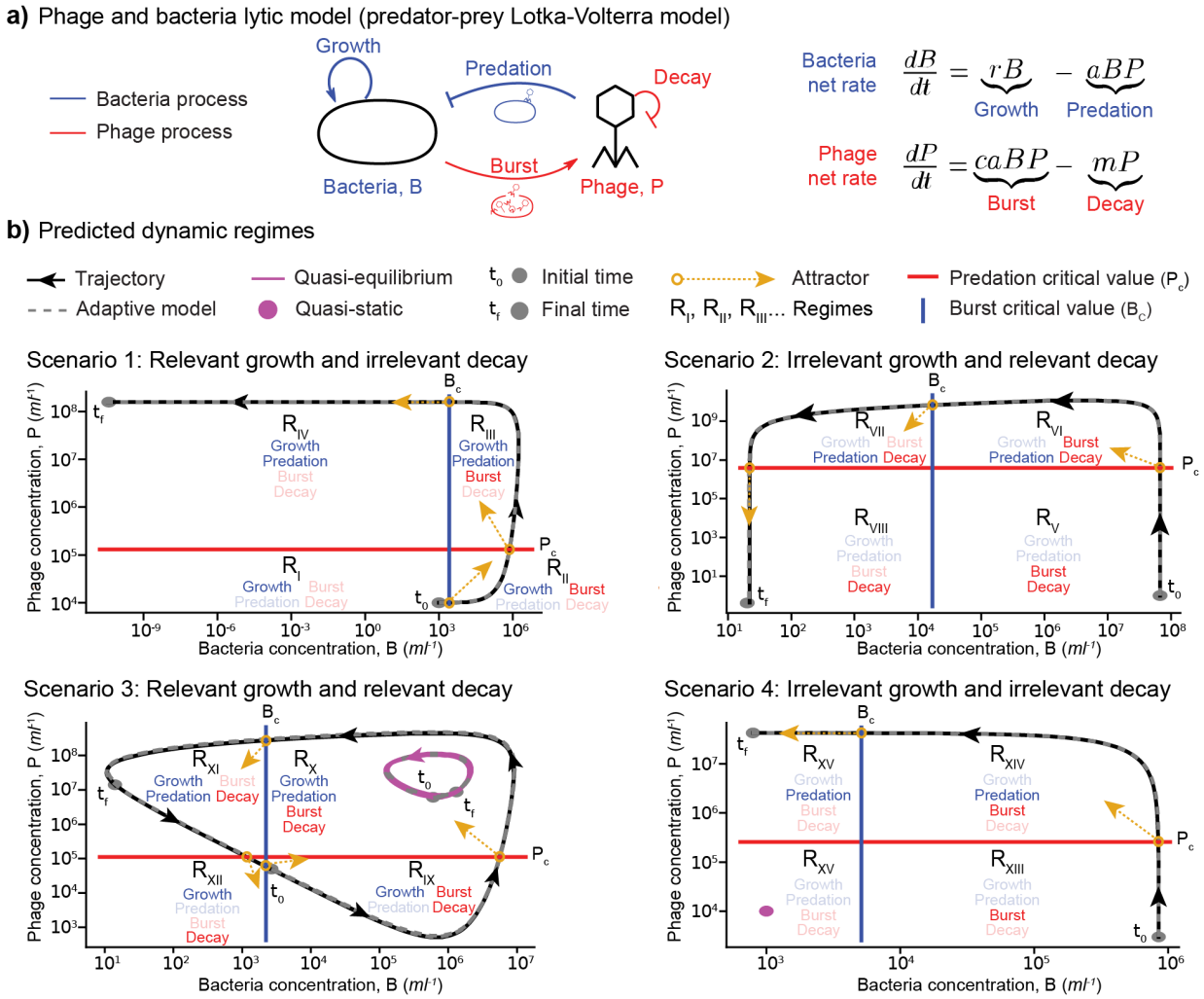

Figure 2. Dynamic regimes for a phage and bacteria lytic model. a) Diagram displaying the processes impacting the bacteria, B (blue) and phage, P (red) populations. The mathematical terms of each process are displayed in the net rate change of each population, respectively, *dB/dt* and *dP/dt*. The parameters are *r* (growth rate constant), *a* (adsorption-infection rate constant), *c* (burst size), and *m* (decay rate constant). **b)** Dynamic regimes, R_i, for the four scenarios predicted based on the observational principle-based transient dynamics analysis and determined by either the bacterial growth process or phage decay process being either relevant or irrelevant. Each plot displays the phage concentration versus the bacteria concentration (black curve), with the black arrows indicating the time direction. The grey dots are the initial and end times. The magenta curves display quasi-equilibrium and quasi-static trajectories. The vertical (blue) and horizontal (red) lines represent the critical concentrations of bacteria (B_c) and phage (P_c). Each regime (quadrant) displays the labels of the relevant (opaque) and non-relevant (semi-transparent) processes. The dashed grey curves display the approximate trajectories from the adaptive Boolean model, simulating only relevant processes. The parameters for the trajectories are listed in Table 1.

The predator-prey system comprising four processes yielded $2^4 = 16$ dynamic regimes, Eq (2). Since the weights for the growth, w_g, and decay, w_d, were constant in this reference observational

285 framework, it was possible to explore the dynamic regimes in four scenarios (Figure 2b): Scenario 1
286 (relevant growth and irrelevant decay), Scenario 2 (irrelevant growth and relevant decay), Scenario 3
287 (relevant growth and decay), and Scenario 4 (irrelevant growth and decay). The theoretical asymptotic
288 analysis of each regime (dynamic subsystem with a unique set of relevant processes) identified the
289 attractors for each scenario as indicated in Tables S1 (Scenario 1), S2 (Scenario 2), S3 (Scenario 3), and
290 S4 (Scenario 4) in the Supplementary Information (S1. Asymptotic Analysis). The attractor analysis for
291 the different scenarios predicted quasi-equilibrium when either all processes remained relevant (purple
292 trajectory in Scenario 3) or all processes remained irrelevant (purple trajectory in Scenario 4).
293 The numerical exploration of the scenarios illustrated in Figure 2b was associated with different
294 qualitative biological situations as described in Table 1. The weight analysis and error of the
295 observational framework for each scenario are explored below and displayed in Figures 3 (Scenario 1), S1
296 (Scenario 2), 4 (Scenario 3), and S2 (Scenario 4).
297
298 ***Processes predicted to be relevant accurately reproduce transient dynamics.*** The first biological
299 scenario, related to Figure 2b, Scenario 1 (relevant growth and irrelevant decay), was investigated using
300 parameters and observational times consistent with laboratory experiments for fast-growing bacteria, such
301 as *E. coli*, and lytic phages, like T4 phage (Table 1). The observational time was $\tau = 14$ h, and the
302 tolerance for the relevant observational change was 10% of the population ($\alpha = 0.1$). The weight analysis
303 identified four regimes based on the combination of relevant processes (Figure 3a): bacterial growth (R_I),
304 bacterial growth and phage burst (R_{II}), bacterial growth, phage burst, and phage predation (R_{III}), and
305 bacterial growth and phage predation (R_{IV}). The parameters in this scenario predicted a bacterial critical
306 value of $B_c = 2.6 \cdot 10^3$ cells/ml, regulating the phage production (or burst) process, and a phage critical
307 value $P_c = 1.3 \cdot 10^5$ phages/ml, regulating the predation process. These regimes and their associated critical
308 values distilled the dynamics of the full bacteria and phage model (Figure 3b top). The bacterial
309 population initially increased exponentially, driven by bacterial growth, while the phage population
310 remained relatively constant. The crossing of the critical bacteria concentration ($B > B_c$) at 1.06 h made

the phage burst relevant. The crossing of the phage critical concentration ($P > P_c$) at 7.48 h rendered phage predation relevant, which rapidly outweighed the bacterial growth ($w_b >> w_g = 126$). This yielded a rapid decline of bacteria, which crossed back its critical concentration ($B < B_c$) at 9.90 h, making the burst process irrelevant and stalling the phage production, which remained relatively constant because the phage decay process remained irrelevant throughout the dynamics. The dynamics of the adaptive Boolean model, which integrated only relevant processes ($w > w_{th}$), were visually indistinguishable from those of the full model (Figure 3b top). The error analysis indicated that the accuracy varied across the regimes, yielding an average relative error (combined populations) of 2.26% (Figure 3b bottom), with the bacterial population's most significant error in the fourth regime (mean error = 10.87%) and the phage in the third regime (mean error = 2.60%) (see S4. Relative Error).

The opposite transient dynamic scenario, that is, one with irrelevant bacterial growth and relevant phage decay, as shown in Figure 2b (Scenario 2), utilized parameters related to marine systems, featuring slow-growing bacteria and fast phage decay occurring at the sea surface due to sunlight effects (see Table 1). The observational time was $\tau = 300$ h (nearly two weeks), and the tolerance to change was again 10% ($\alpha = 0.1$). The parameters used yielded the critical values $B_c = 1.48 \cdot 10^4$ cells/ml and $P_c = 3.3 \cdot 10^6$ phages/ml for bacteria and phage, respectively. The weight and trajectory dynamic analysis captured four expected regimes (Figure S1): R_V (burst and decay), R_{VI} (predation, burst, and decay), R_{VII} (predation and decay), and R_{VIII} (decay). The phage production initially outweighed the decay, resulting in a rapid increase in phage that caused the decline of the bacteria. After the bacterial population crossed its critical point, the phage burst became irrelevant, resulting in an exponential decay of the phage. The phage adaptive Boolean model yielded a mean (combined) error of 0.42% with maximum errors of 0.76% for bacteria and 0.31% for phage (see S4. Relative Error).

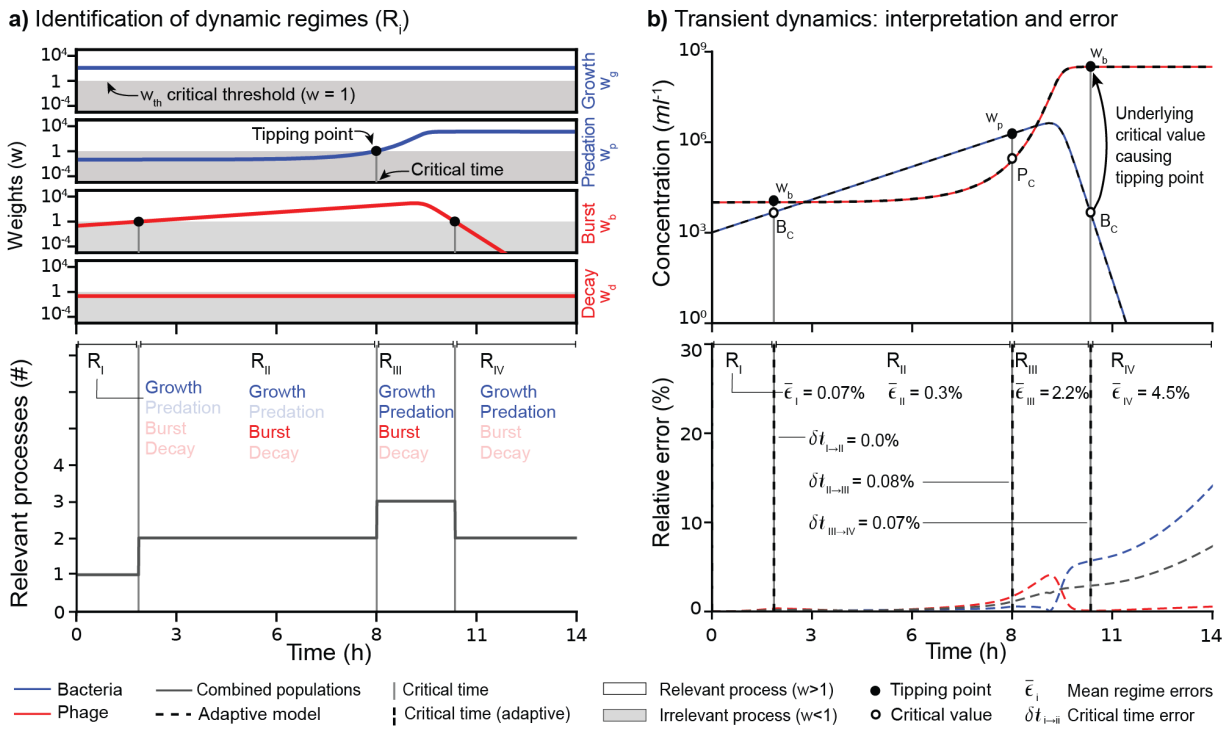

Figure 3. Transient dynamics analysis using the finite observational framework. Dynamic regimes and transient dynamics interpretation for the scenario with relevant growth ($w_g>1$) and irrelevant decay ($w_d<1$), corresponding to Scenario 1 in Figure 2. The model parametrization is shared in Table 1. **a)** The dimensionless weights for each process (top panel) and the number of relevant processes (bottom panel) are plotted as a function of the observed time. Processes associated with bacteria are displayed in blue and those for the phage in red. The white region in the weights indicates when processes are relevant, above the critical threshold ($w>w_{th} = 1$). The grey region displays when processes are irrelevant. Black circles indicate tipping points, and vertical grey lines indicate the critical times, separating regimes, R_i. **b)** The dynamics for the bacteria (blue) and phage (red) over time (top panel) are compared with the relative error of the adaptive Boolean model (bottom panel). The dashed curves and vertical lines represent the predictions from the adaptive model, which simulated only relevant processes. The mean relative errors for each regime, $\bar{\epsilon}_i$, and the error in the critical time transitions, $\delta t_{i\to ii}$, are displayed.

Two observable quasi-equilibrium regimes in the Lotka-Volterra dynamics. The quasi-equilibrium dynamic predicted when all processes were relevant (Table S3) was recovered in Scenario 3. The parameters for Scenario 3 were similar to those for the marine populations in Scenario 2, but assuming a faster-growing bacterial population, which is possible in enriched environments such as inhabited coastal ecosystems (Table 1). The observational time was again τ = 300 h (nearly two weeks), and the tolerance to change was again 10% (α = 0.1). The parameters used yielded the critical values $B_c = 2.2\cdot10^3$ cells/ml and $P_c = 1.1\cdot10^5$ phages/ml for bacteria and phage, respectively. The initial conditions were above the critical concentrations for both bacteria and phage, and the constant weights, growth (w_g) and decay (w_d)

(see Eq. 3), where of the same order, $\frac{w_g}{w_d} = \frac{r}{m} \approx 1$, due to similar values of the rate constant (r) and decay rate constant (m) (Table 1, Scenario 1). These two conditions yielded oscillations around the classical theoretical equilibrium of the Lotka-Volterra system for bacteria and phage, respectively, $B_{eq} = \frac{m}{c \cdot a} \approx 6.7 \cdot 10^5$ cells/ml and $P_{eq} = \frac{r}{a} \approx 3.3 \cdot 10^7$ phages/ml with all processes remaining relevant throughout the dynamics (Figure 4a), resulting in no errors in the adaptive Boolean model (see S4. Relative Error).

Initial conditions where at least one of the populations was below the critical concentration were predicted to make one of the variable processes (predation or burst) initially irrelevant. The conditions used in this case rendered the predation initially irrelevant and fueled transient dynamics that alternated between four regimes (Figure 4b, left): R_{IX} (growth, burst, and decay), R_X (all relevant), R_{XI} (growth, predation, and decay), and R_{XII} (growth and decay). The phage and bacterial populations oscillated abruptly, crossing their critical concentrations repeatedly (Figure 4b, right), which was associated with the broader cycle in the phase diagram (Figure 2b, Scenario 3). The adaptive Boolean model, which integrated only relevant processes, accurately reproduced the dynamics of the full model (Figure 4b, right). The mean combined error was 0.74%, and the errors in the bacterial and phage populations increased locally during the short regimes with abrupt population changes (Figure 4b, right-bottom).

The second quasi-equilibrium situation was predicted when all processes were irrelevant, resulting in all populations remaining quasi-static (Table S4). This prediction was captured in the case with irrelevant growth and decay, corresponding to Scenario 4 (Figure 2b, purple trajectory). The parameters used resembled the environmental values of Scenario 2, using slow phage decay instead, a plausible situation in the deep ocean (Table 1). The observational time was shortened to be similar to laboratory conditions τ = 13 h, as in Scenario 1. The tolerance to change was again 10% (α = 0.1). The critical concentrations were $B_c = 5.1 \cdot 10^3$ cells/ml and $P_c = 2.6 \cdot 10^5$ phages/ml for phage. Initial conditions below the critical values ($B_0 = 1 \cdot 10^{\wedge 3}$ cells/ml < B_c and $P_0 = 1 \cdot 10^{\wedge 4}$ phages/ml < P_c) rendered all processes irrelevant, yielding relatively constant concentrations of phage and bacteria for the observer. The adaptive Boolean model yielded a combined average error of 0.09% (see S4. Relative Error). Using

initial conditions above the critical bacterial concentration ($B_0 = 8.5 \cdot 10^{\wedge 3}$ cells/ml > B_c) made the burst process relevant (Figure S2a). This increased the phage concentration and eventually decimated the bacterial population below the critical concentration (Figure S2b). The adaptive model for relevant processes yielded an error of 2.06% with respect to the full model (Figures S2b and S4. Relative Error).

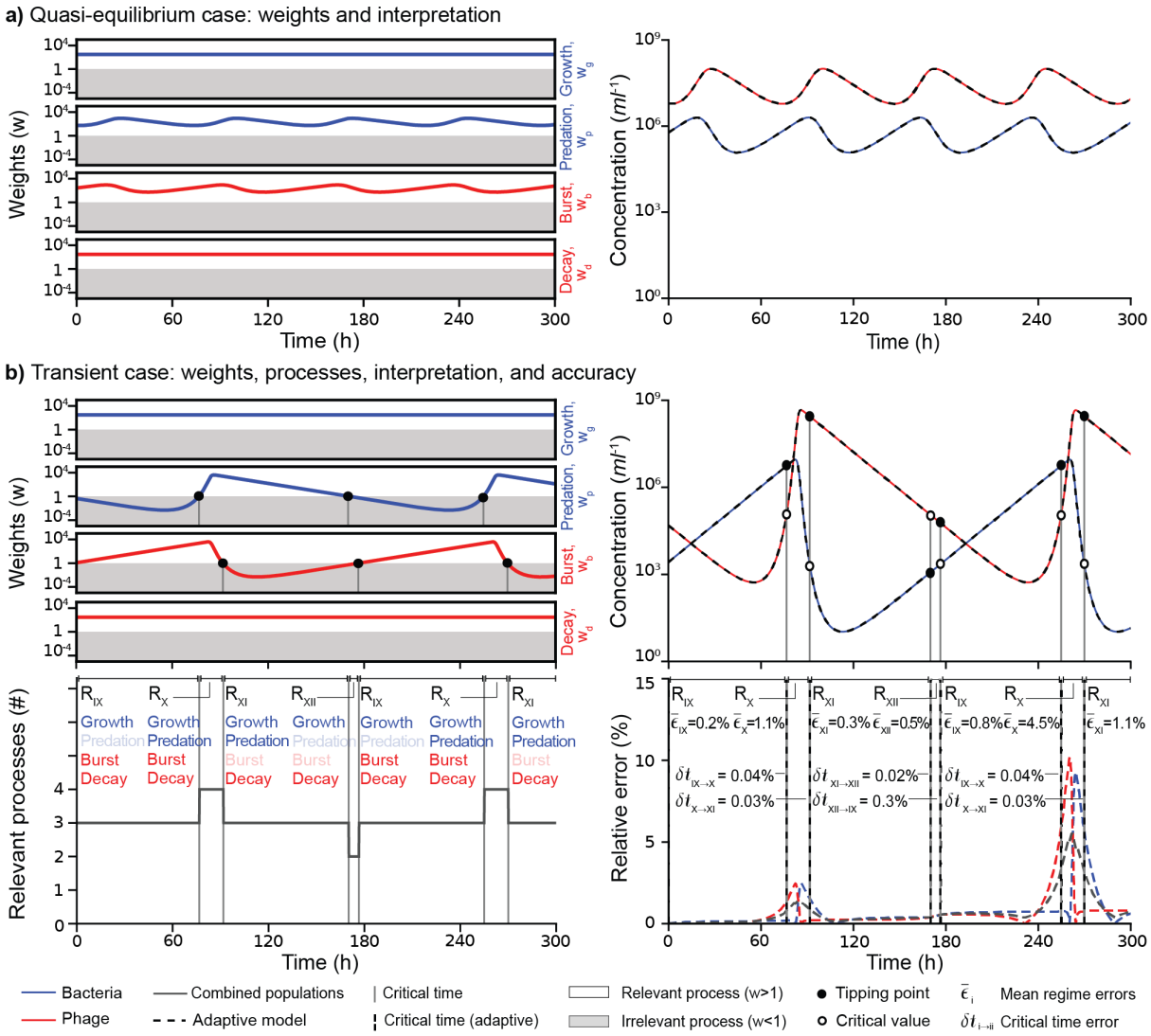

Figure 4. Scenario displaying quasi-equilibrium. Dynamics in the scenario with relevant growth ($w_g>1$) and irrelevant decay ($w_d<1$), corresponding to Scenario 3 in Figure 2. The model parametrization is shared in Table 1. The color coding and symbols are analogous to Figure 3. **a)** The left panel displays the weights for phage (blue) and bacterial (red) processes over time. The right panel shows the dynamics of phage and bacterial concentrations. The dashed lines correspond to the adaptive Boolean model. No error plot is included because all processes remained relevant. **b)** The top two plots are analogous to those in **a),** but with initial conditions that lead to transient dynamics. The bottom plots include the relevant process over time (left) and the relative error of the adaptive Boolean model (right). The solid circles indicate tipping points, and the vertical lines indicate critical times. The mean relative errors for each regime, $\bar{\epsilon}_i$, and the error in the critical time transitions, $\delta t_{i\to ii}$, are displayed. The dynamic regimes, R_i, are displayed in both bottom panels following the same notations as in Figure 2.

The observational framework accurately predicts when new processes matter.

The bacterial competition process $-\frac{rB^2}{K}$, where K was the carrying capacity, was added to the phage and bacteria model (Figure 5a). This term introduced an asymptotically globally stable equilibrium $B_{eq} = \frac{m}{c \cdot a}$ and $P_{eq} = \frac{r}{a} \cdot \left(1 - \frac{B_{eq}}{K}\right)$. The observational framework predicted that the effect should be only observable if its weight $w_K = \frac{\tau\, r\, B^2}{\alpha\, K}$ was relevant ($w_K > w_{th} = 1$). This was tested using the conditions for quasi-equilibrium from Scenario 3 and setting up the carrying capacity to $K = 10^9 \frac{cells}{ml}$, a reasonable upper value in coastal conditions (Table 1). These conditions yielded a carrying capacity weight below the threshold $w_K = 0.18 < w_{th} = 1$, and the carrying capacity process remained irrelevant throughout the dynamics (Figure 5b). The system, thus, displayed the periodic quasi-equilibrium oscillations already observed in the initial model (Figures 4a and 5b). The adaptive Boolean model produced a dynamic that was visually indistinguishable from the full model that contained the carrying capacity and yielded a mean combined error of 1.0% (Figure 5b and S4. Relative Error). The observational framework predicted that the observational time would have to be $\tau' \geq \tau_0' = \frac{K * \alpha}{r * B}$ for the carrying capacity to be relevant. Applying the equilibrium value for the bacteria concentration yielded $\tau_0' \approx 10{,}000\ h$ (over a year). The observational time used was about three times larger $\tau' = 30{,}000\ h > \tau_0'$. This yielded dynamics where all processes were relevant (Figure 5c). The amplitudes of the oscillations started to dampen and converge toward the asymptotic global stable equilibrium at the predicted time $\tau_0' \approx 10{,}000\ h$ t (Figure 5c). The adaptive Boolean model yielded no errors because all processes were relevant.

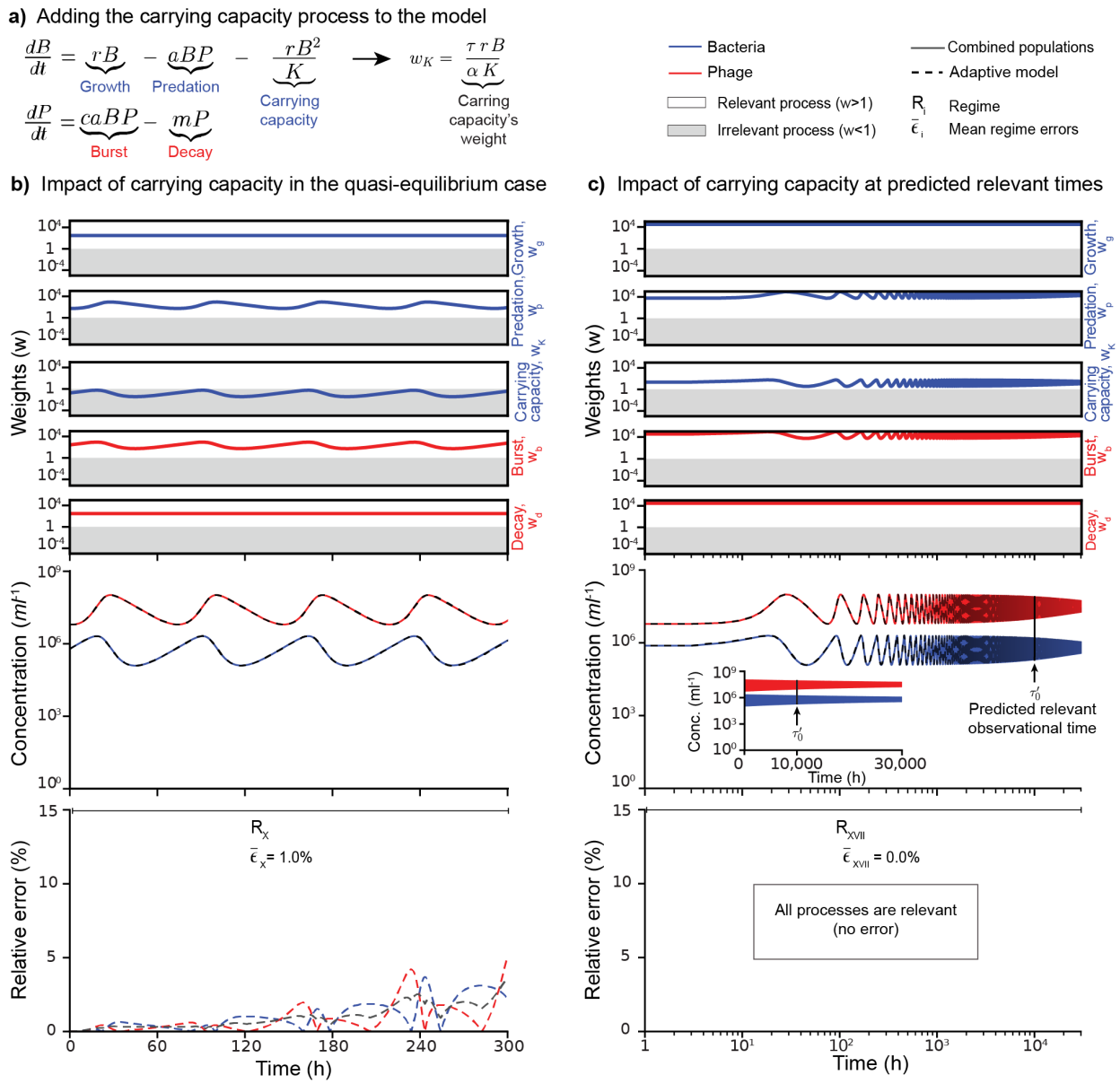

Figure 5. Impact of adding a new process to the dynamics: the carrying capacity. The original model was modified to include the carrying capacity process, which limits bacterial growth. The model parametrization is shared in Table 1. **a)** Phage and bacteria model including the carrying capacity. Each process is labeled. The weight of the carrying capacity process is displayed, w_K. The color coding and symbols in this figure are analogous to Figures 2 to 4; the subset used is displayed to the right. **b)** Transient dynamic analysis for the same quasi-equilibrium case (relevant growth and decay, Scenario 3) displayed in Figure 4a. The plot for the weights includes the carrying capacity process. The population dynamics of phage (red) and bacteria (blue) and the adaptive model's (dashed lines) error are plotted. The regime and mean error are displayed. **c)** Transient dynamics for the same case as in **b)** but for a larger observational time. The time is displayed on a logarithmic scale. The inset plot displays the time on a linear scale. The vertical arrows indicate the predicted relevant time, τ_0', to observe the impact of the carrying capacity.

DISCUSSION

The application of the finite observational framework introduced here illustrates how a system with a limited number of underlying processes, such as the standard predator-prey Lotka-Volterra system, can display a wide range of dynamical regimes for a real observer (Figure 2). The fourteen transient regimes and two quasi-equilibrium regimes characterized in this system contrast with the classic asymptotic analysis of the Lotka-Volterra model, which expects a periodic solution and a trivial (null concentrations) equilibrium (Murray, 2007; Weitz, 2016). A real observer, instead, would perceive the classic periodic solution only when all four processes (growth, predation, burst, and decay) are relevant throughout the observational time (Figure 2 and Figure 4). This makes the conditions for quasi-equilibrium a far more stringent set of conditions than in the classic analysis. The concentrations of both agents must remain within values close enough to the critical concentrations, so the amplitudes of the oscillations do not cross any tipping points (Figure 4).

The finite observable framework also predicts scenarios that are not captured in the classic asymptotic analysis, such as the existence of a quasi-static solution when the processes are not relevant (Figure 2) or when a potential additional process, like the carrying capacity, remains irrelevant (Figure 5). Most of these transient regimes, predicted and measured within the finite observable framework, would not have been accessible using published methods for transient dynamics. Inference methods that rely on data would not be able to predict the drastic effects of a new process becoming relevant with a trajectory where its weights until that moment would be negligible within the observer's tolerance (Boettiger & Hastings, 2012; Bury et al., 2021). The transient dynamics methods that rely on asymptotic assumptions, such as those based on critical transitions, would also be ineffective in recovering the dynamic transitions described here because they assume that the transitions are due to attractors that change the trajectories between stable regimes (Hastings et al., 2018; Scheffer, 2009; Scheffer et al., 2009). The sloppy model approach could identify that some of the processes are irrelevant, but its underlying dependency on asymptotic manifolds would overlook the fact that some processes can transition from irrelevant to relevant and vice versa (Gutenkunst et al., 2007). The research presented here demonstrates instead that

454 the local attractors associated with relevant processes at a given time drive the dynamics until a tipping
455 point is crossed, altering the set of relevant processes (Figure 2 and Table S1). This also supports the
456 drastic effect that local events can have globally on a system (Albert & Barabási, 2000; Strogatz, 2001).
457 The transient regimes are measurable for an observer, as demonstrated by the fact that the
458 adaptive Boolean model, which simulates only relevant processes, accurately reproduced the dynamics
459 (Figure 2 and S4. Relative Error). These regimes provide a guide for distilling specific systems, as seen in
460 the case study on phage and bacteria investigated here. If the life traits (model parameters) of a bacterial
461 host and phage pair, along with their initial concentrations, do not fall within the stringent ranges for
462 quasi-equilibrium, transient dynamics are expected. The exploration of the empirical parameter ranges
463 suggests that the lytic lifestyle should lead to phage-host pair dynamics that are transient and often far
464 from the quasi-equilibrium scenario (Figure 2). Community effects, such as the evolution of virus-host
465 (predator-prey) networks (Castledine & Buckling, 2024; Flores et al., 2011; Holt, 1977; Koskella &
466 Brockhurst, 2014; Thingstad, 2000, 2022; Våge et al., 2013; Varona et al., 2024), holobiont networks
467 ((Barott & Rohwer, 2012; Roughgarden, 2023), and alternative lifestyles, like lysogeny, where the virus
468 integrates into the host (Howard-Varona et al., 2017; Kimchi et al., 2024; Knowles et al., 2016;
469 Roughgarden, 2024; Silveira et al., 2021), are likely responsible for the diverse range of stable
470 concentrations of viruses and bacteria observed in microbial communities across ecosystems (Anthenelli
471 et al., 2020; Luque & Silveira, 2020; Parikka et al., 2016; Wigington et al., 2016). The identification of
472 relevant processes depending on the parameter ranges can help simplify theoretically driven approaches
473 to phage therapy(Cairns et al., 2009; Levin et al., 2024; Levin & Bull, 2004; Roach et al., 2017).
474 A key advantage of the framework introduced here is that the calculations are relatively simple,
475 yielding a practical recipe for obtaining conditions associated with tipping points (Figure 1). The case
476 investigated here involved only four processes, making it feasible to explore the sixteen (2^4) dynamic
477 regimes predicted (Figure 2 and Table S1). However, the number of potential dynamic regimes increases
478 exponentially with the number of processes in the system (Eq. 2), so describing all possible dynamics in
479 most systems is unfeasible. The practical advantage of the framework lies in its ability to identify the

essential processes in each context and indicate the conditions under which a process becomes relevant or irrelevant throughout the dynamics, thereby altering the system's trajectory. This knowledge also provides information on how to characterize or engineer the dynamics of complex systems that could simplify ongoing efforts (Gilman et al., 2010; Kauffman, 1995; Kondor et al., 2023; Kortessis et al., 2025; Panahi et al., 2023; Strogatz, 2001; Turchin, 2003). A limitation of the framework introduced in this formulation is the requirement of prior knowledge regarding the potential processes involved in a system, along with their corresponding parameter ranges. Nonetheless, the concept of weights and finite constraints could be extended to assess the contribution of processes inferred in machine learning and data-driven methods (Guimerà et al., 2020).

Finally, the observational framework reveals an inherent subjectivity that is often overlooked in sciences (Kuhn, 2012; Zimring, 2019). The perception and interpretation of the dynamics depend on the context of the observer, such as the observational time (Figure 1). Dynamical systems may exhibit well-defined asymptotic characteristics that can be considered universal mathematically, like the global stability introduced by the carrying capacity (Jasien, 2017; So, 1979). Yet observers, whose perception is finite, do not have access to such universal properties. They instead live in local dynamics that may lead to very different perceptions of the system, as exemplified in the case of the observers describing the phage and bacteria dynamics over either the two-week or two-month period (Figure 5). The former would describe the system as periodically driven by the four standard processes in the Lotka-Volterra dynamics, while the latter would perceive the long-term effect of the carrying capacity, which smooths the oscillations of the system. In their contexts, both descriptions are accurate and relevant. The extrapolation of this result indicates that, in more complex scenarios, the dynamics observed may often be associated with a small number of relevant processes that dominate, providing a theoretical foundation for the prevalence of the Pareto Principle (80/20 rule), principle of factor sparsity across systems, self-organization, and apparent simplicity in complex systems (Cooper et al., 2019; Garte et al., 2025; Kauffman, 1995; McCarthy & Winer, 2018; Quinn et al., 2023; Strogatz, 2001).

CONCLUSION

The observational framework introduced here is a pragmatic and accurate approach to forecasting tipping points and regime shifts in dynamical systems. It builds on the foundational empirical principle that observers are subject to finite measurements. This principle leads to reference observational rates that determine when processes are relevant, contributing to the attractors that drive the dynamics perceived by the observer. Tipping points occur when dynamic processes become relevant or irrelevant to the observer, thereby changing the attractor that steers the system. The different combinations of relevant processes generate a rich range of transient and a few quasi-stable dynamic regimes that are observable but overlooked in classic asymptotic approaches. The observational framework thus indicates that dynamic regimes and tipping points depend on the observer's context and highlights the need to use the observer's finite perception as the cornerstone element in the description and forecasting of dynamical systems.

ACKNOWLEDGEMENTS

The authors thank Joan Roughgarden, the Biomath working group at San Diego State University, and Alexander V. Alekseyenko (Medical University of South Carolina) for their invaluable insights and fruitful discussions throughout the project. The authors also acknowledge the crucial influence of the Master's Thesis from Matthew C. Witt, carried out under the supervision of Antoni Luque at San Diego State University (Witt, 2019), and the theoretical inspiration from several key references (Cairns et al., 2009; Hastings et al., 2018; Scheffer, 2009; Turchin, 2003). The authors acknowledge the funding support of different agencies that made the research published here possible. The National Science Foundation award #2424579 supported the research of A.L. and L.J.C. The Gordon and Betty Moore Foundation grant GBMF9871 (https://doi.org/10.37807/GBMF9871) supported the research of A.L. and F.R. The Gordon and Betty Moore Foundation grant GBMF9207 (https://doi.org/10.37807/GBMF9207) supported the research of S.C.-L. and F.R. The Margarita Salas Grant for the training of young doctors 2021URV-MS-20 supported the research of S.C.-L.

REFERENCES

Albert, R., & Barabási, A.-L. (2000). Topology of Evolving Networks: Local Events and Universality. *Physical Review Letters*, *85*(24), 5234–5237. https://doi.org/10.1103/PhysRevLett.85.5234

Anthenelli, M., Jasien, E., Edwards, R., Bailey, B., Felts, B., Katira, P., Nulton, J., Salamon, P., Rohwer, F., Silveira, C. B., & Luque, A. (2020). Phage and bacteria diversification through a prophage acquisition ratchet. *BioRxiv*, *April*. https://doi.org/https://doi.org/10.1101/2020.04.08.028340

Barott, K. L., & Rohwer, F. L. (2012). Unseen players shape benthic competition on coral reefs. *Trends in Microbiology*, *20*(12), 621–628. https://doi.org/10.1016/J.TIM.2012.08.004

Bashkirtseva, I., & Ryashko, L. (2018). Stochastic Sensitivity Analysis of Noise-Induced Extinction in the Ricker Model with Delay and Allee Effect. *Bull Math Biol*, *80*(6), 1596–1614. https://doi.org/10.1007/s11538-018-0422-6

Battistel, L., Vilardi, A., Zampini, M., & Parin, R. (2023). An investigation on humans' sensitivity to environmental temperature. *Scientific Reports*, *13*(1), 21353. https://doi.org/10.1038/s41598-023-47880-5

Boettiger, C., & Hastings, A. (2012). Quantifying limits to detection of early warning for critical transitions. *Journal of The Royal Society Interface*, *9*(75), 2527–2539. https://doi.org/10.1098/rsif.2012.0125

Brum, J. R., Hurwitz, B. L., Schofield, O., Ducklow, H. W., & Sullivan, M. B. (2016). Seasonal time bombs: dominant temperate viruses affect Southern Ocean microbial dynamics. *The ISME Journal*, *10*(2), 437–449. https://doi.org/10.1038/ismej.2015.125

Bury, T. M., Sujith, R. I., Pavithran, I., Scheffer, M., Lenton, T. M., Anand, M., & Bauch, C. T. (2021). Deep learning for early warning signals of tipping points. *Proceedings of the National Academy of Sciences*, *118*(39), e2106140118. https://doi.org/doi:10.1073/pnas.2106140118

Cairns, B. J., Timms, A. R., Jansen, V. A. A., Connerton, I. F., & Payne, R. J. H. (2009). Quantitative Models of In Vitro Bacteriophage–Host Dynamics and Their Application to Phage Therapy. *PLOS Pathogens*, *5*(1), e1000253. https://doi.org/10.1371/journal.ppat.1000253

Castledine, M., & Buckling, A. (2024). Critically evaluating the relative importance of phage in shaping microbial community composition. *Trends in Microbiology*, *32*(10), 957–969. https://doi.org/10.1016/j.tim.2024.02.014

Cheng, H., Zhang, H., Spötl, C., Baker, J., Sinha, A., Li, H., Bartolomé, M., Moreno, A., Kathayat, G., Zhao, J., Dong, X., Li, Y., Ning, Y., Jia, X., Zong, B., Ait Brahim, Y., Pérez-Mejías, C., Cai, Y., Novello, V. F., … Edwards, R. L. (2020). Timing and structure of the Younger Dryas event and its underlying climate dynamics. *Proceedings of the National Academy of Sciences*, *117*(38), 23408–23417. https://doi.org/doi:10.1073/pnas.2007869117

Cheng, K., Zhao, Y., Du, X., Zhang, Y., Lan, S., & Zhengli, S. (2007). Solar radiation-driven decay of cyanophage infectivity, and photoreactivation of the cyanophage by host cyanobacteria. *Aquatic Microbial Ecology*, *48*, 13–18. https://doi.org/10.3354/ame048013

Clements, C. F., McCarthy, M. A., & Blanchard, J. L. (2019). Early warning signals of recovery in complex systems. *Nature Communications*, *10*(1), 1681. https://doi.org/10.1038/s41467-019-09684-y

Cooper, L., Kang, S. Y., Bisanzio, D., Maxwell, K., Rodriguez-Barraquer, I., Greenhouse, B., Drakeley, C., Arinaitwe, E., G. Staedke, S., Gething, P. W., Eckhoff, P., Reiner, R. C., Hay, S. I., Dorsey, G., Kamya, M. R., Lindsay, S. W., Grenfell, B. T., & Smith, D. L. (2019). Pareto rules for malaria super-spreaders and super-spreading. *Nature Communications*, *10*(1), 3939. https://doi.org/10.1038/s41467-019-11861-y

Cushing, J., Dennis, B., Desharnais, R., & Costantino, R. (1998). Moving toward an unstable equilibrium: saddle nodes in population systems. *Journal of Animal Ecology*, *67*(2), 298–306. https://doi.org/10.1046/j.1365-2656.1998.00194.x

Dakos, V., Boulton, C. A., Buxton, J. E., Abrams, J. F., Arellano-Nava, B., Armstrong McKay, D. I., Bathiany, S., Blaschke, L., Boers, N., Dylewsky, D., López-Martínez, C., Parry, I., Ritchie, P., van der Bolt, B., van der Laan, L., Weinans, E., & Kéfi, S. (2024). Tipping point detection and early warnings in climate, ecological, and human systems. *Earth System Dynamics*, *15*(4), 1117–1135. https://doi.org/10.5194/esd-15-1117-2024

De Paepe, M., & Taddei, F. (2006). Viruses' Life History: Towards a Mechanistic Basis of a Trade-Off between Survival and Reproduction among Phages. *PLoS Biology*, *4*(7), e193. https://doi.org/10.1371/journal.pbio.0040193

Ditlevsen, P., & Ditlevsen, S. (2023). Warning of a forthcoming collapse of the Atlantic meridional overturning circulation. *Nature Communications*, *14*(1), 4254. https://doi.org/10.1038/s41467-023-39810-w

Flores, C. O., Meyer, J. R., Valverde, S., Farr, L., & Weitz, J. S. (2011). Statistical structure of host–phage interactions. *Proceedings of the National Academy of Sciences*, *108*(28), E288–E297. https://doi.org/10.1073/pnas.1101595108/-/DCSupplemental.www.pnas.org/cgi/doi/10.1073/pnas.1101595108

Garte, S., Marshall, P., & Kauffman, S. (2025). The Reasonable Ineffectiveness of Mathematics in the Biological Sciences. *Entropy*, *27*(3), 280. https://doi.org/10.3390/e27030280

Gilman, S. E., Urban, M. C., Tewksbury, J., Gilchrist, G. W., & Holt, R. D. (2010). A framework for community interactions under climate change. *Trends in Ecology & Evolution*, *25*(6), 325–331. https://doi.org/10.1016/j.tree.2010.03.002

Gladwell, M. (2000). *The Tipping Point: How Little Things Can Make a Big Difference* (First edition). Little Brown.

Guimerà, R., Reichardt, I., Aguilar-Mogas, A., Massucci, F. A., Miranda, M., Pallarès, J., & Sales-Pardo, M. (2020). A Bayesian machine scientist to aid in the solution of challenging scientific problems. *Science Advances*, *6*(5). https://doi.org/10.1126/sciadv.aav6971

Gutenkunst, R. N., Waterfall, J. J., Casey, F. P., Brown, K. S., Myers, C. R., & Sethna, J. P. (2007). Universally Sloppy Parameter Sensitivities in Systems Biology Models. *PLoS Computational Biology*, *3*(10), e189. https://doi.org/10.1371/journal.pcbi.0030189

Haas, A. F., Fairoz, M. F. M., Kelly, L. W., Nelson, C. E., Dinsdale, E. A., Edwards, R. A., Giles, S., Hatay, M., Hisakawa, N., Knowles, B., Lim, Y. W., Maughan, H., Pantos, O., Roach, T. N. F., Sanchez, S. E., Silveira, C. B., Sandin, S., Smith, J. E., & Rohwer, F. (2016). Global microbialization of coral reefs. *Nature Microbiology*, *April*, 16042. https://doi.org/10.1038/nmicrobiol.2016.42

Hastings, A., Abbott, K. C., Cuddington, K., Francis, T., Gellner, G., Lai, Y.-C., Morozov, A., Petrovskii, S., Scranton, K., & Zeeman, M. Lou. (2018). Transient phenomena in ecology. *Science*, *361*(6406), eaat6412. https://doi.org/doi:10.1126/science.aat6412

Hindmarsh, A. C. (1983). *ODEPACK, A Systematized Collection of ODE Solvers,* (R. S. Stepleman, M. Carver, R. Peskin, W. F. Ames, & R. Vichnevetsky, Eds.; Vol. 1, pp. 55–64). Scientific Computing.

Holt, R. D. (1977). Predation, apparent competition, and the structure of prey communities. *Theoretical Population Biology*, *12*(2), 197–229. https://doi.org/10.1016/0040-5809(77)90042-9

Howard-Varona, C., Hargreaves, K. R., Abedon, S. T., & Sullivan, M. B. (2017). Lysogeny in nature: mechanisms, impact and ecology of temperate phages. *The ISME Journal*, 1–10. https://doi.org/10.1038/ismej.2017.16

Jasien, E. (2017). *Modeling the Transition Between Lytic and Lysogenic Behavior in a Bacteria-Phage System* [Master]. San Diego State University.

Jiang, J., Huang, Z.-G., Seager, T. P., Lin, W., Grebogi, C., Hastings, A., & Lai, Y.-C. (2018). Predicting tipping points in mutualistic networks through dimension reduction. *Proceedings of the National Academy of Sciences*, *115*(4). https://doi.org/10.1073/pnas.1714958115

Kannoly, S., Oken, G., Shadan, J., Musheyev, D., Singh, K., Singh, A., & Dennehy, J. J. (2023). Single-Cell Approach Reveals Intercellular Heterogeneity in Phage-Producing Capacities. *Microbiology Spectrum*, *11*(1). https://doi.org/10.1128/spectrum.02663-21

Kauffman, S. (1995). *At home in the universe: The search for laws of self-organization and complexity* (1st ed.). Oxford University Press, USA.

Kevorkian, J., & Cole, J. D. (1981). Limit Process Expansions Applied to Ordinary Differential Equations. In J. Kevorkian & J. D. Cole (Eds.), *Perturbation Methods in Applied Mathematics* (pp. 17–104). Springer New York. https://doi.org/10.1007/978-1-4757-4213-8_2

Kimchi, O., Meir, Y., & Wingreen, N. S. (2024). Lytic and temperate phage naturally coexist in a dynamic population model. *The ISME Journal*, *18*(1). https://doi.org/10.1093/ismejo/wrae093

Knowles, B., Silveira, C. B., Bailey, B. A., Barott, K., Cantu, V. A., Cobian-Guëmes, A. G., Coutinho, F. H., Dinsdale, E. A., Felts, B., Furby, K. A., George, E. E., Green, K. T., Gregoracci, G. B., Haas, A. F., Haggerty, J. M., Hester, E. R., Hisakawa, N., Kelly, L. W., Lim, Y. W., … Rohwer, F. (2016). Lytic to temperate switching of viral communities. *Nature*, *531*(7595), 466–470. https://doi.org/10.1038/nature17193

Kondor, D., Bennett, J. S., Gronenborn, D., Antunes, N., Hoyer, D., & Turchin, P. (2023). Explaining population booms and busts in Mid-Holocene Europe. *Scientific Reports*, *13*(1), 9310. https://doi.org/10.1038/s41598-023-35920-z

Kortessis, N., Glass, G., Gonzalez, A., Ruktanonchai, N. W., Simon, M. W., Singer, B., & Holt, R. D. (2025). Metapopulations, the Inflationary Effect, and Consequences for Public Health. *The American Naturalist*, *205*(3), 342–359. https://doi.org/10.1086/733896

Koskella, B., & Brockhurst, M. A. (2014). Bacteria–phage coevolution as a driver of ecological and evolutionary processes in microbial communities. *FEMS Microbiology Reviews*, *38*(5), 916–931. https://doi.org/10.1111/1574-6976.12072

Kuhn, T. S. (2012). *The structure of scientific revolutions: 50th anniversary* (4th ed.). University of Chicago Press.

Levin, B. R., Berryhill, B. A., Gil-Gil, T., Manuel, J. A., Smith, A. P., Choby, J. E., Andersson, D. I., Weiss, D. S., & Baquero, F. (2024). Theoretical considerations and empirical predictions of the pharmaco- and population dynamics of heteroresistance. *Proceedings of the National Academy of Sciences*, *121*(16). https://doi.org/10.1073/pnas.2318600121

Levin, B. R., & Bull, J. J. (2004). Population and evolutionary dynamics of phage therapy. *Nature Reviews Microbiology*, *2*(2), 166–173. https://doi.org/10.1038/nrmicro822

Luque, A., & Silveira, C. B. (2020). Quantification of lysogeny caused by phage coinfections in microbial communities from biophysical principles. *MSystems*, *5*, e00353-20. https://doi.org/10.1128/mSystems.00353-20

Lyons, T. W., Reinhard, C. T., & Planavsky, N. J. (2014). The rise of oxygen in Earth's early ocean and atmosphere. *Nature*, *506*(7488), 307–315. https://doi.org/10.1038/nature13068

Mao, J., Griniasty, I., Teoh, H. K., Ramesh, R., Yang, R., Transtrum, M. K., Sethna, J. P., & Chaudhari, P. (2024). The training process of many deep networks explores the same low-dimensional manifold. *Proceedings of the National Academy of Sciences*, *121*(12). https://doi.org/10.1073/pnas.2310002121

Margulis, L., & Sagan, D. (1997). *Microcosmos: Four Billion Years of Microbial Evolution*. University of California Press. https://books.google.com/books?id=eo_sMMRxgAUC

McCarthy, D., & Winer, R. S. (2018). The Pareto Rule in Marketing Revisited. *SSRN Electronic Journal*. https://doi.org/10.2139/ssrn.3264425

McLeod, M. J., Barwell, S. A. E., Holyoak, T., & Thorne, R. E. (2025). A structural perspective on the temperature dependent activity of enzymes. *Structure*, *33*(5), 924-934.e2. https://doi.org/10.1016/j.str.2025.02.013

Murray, J. D. (2007). *Mathematical Biology: I. An Introduction* (3rd ed.). Springer.

O'Brien, D. A., Deb, S., Gal, G., Thackeray, S. J., Dutta, P. S., Matsuzaki, S. S., May, L., & Clements, C. F. (2023). Early warning signals have limited applicability to empirical lake data. *Nature Communications*, *14*(1), 7942. https://doi.org/10.1038/s41467-023-43744-8

Oro, D., Alsedà, L., Hastings, A., Genovart, M., & Sardanyés, J. (2023). Social copying drives a tipping point for nonlinear population collapse. *Proceedings of the National Academy of Sciences*, *120*(11), e2214055120. https://doi.org/doi:10.1073/pnas.2214055120

Panahi, S., Do, Y., Hastings, A., & Lai, Y.-C. (2023). Rate-induced tipping in complex high-dimensional ecological networks. *Proceedings of the National Academy of Sciences*, *120*(51), e2308820120. https://doi.org/doi:10.1073/pnas.2308820120

Parikka, K. J., Romancer, M. Le, & Wauters, N. (2016). Deciphering the virus-to-prokaryote ratio (VPR): insights into virus – host relationships in a variety of ecosystems. *Biological Reviews*. https://doi.org/10.1111/brv.12271

Pedersen, E. J., Koen-Alonso, M., & Tunney, T. D. (2020). Detecting regime shifts in communities using estimated rates of change. *ICES Journal of Marine Science*, *77*(4), 1546–1555. https://doi.org/10.1093/icesjms/fsaa056

Petersen, H. A., Miller, E. N., Pham, P. H., Kajal, Katsirubas, J. L., Koltunski, H. J., & Luca, O. R. (2023). On the Temperature Sensitivity of Electrochemical Reaction Thermodynamics. *ACS Physical Chemistry Au*, *3*(3), 241–251. https://doi.org/10.1021/acsphyschemau.2c00063

Petzold, L. (1983). Automatic Selection of Methods for Solving Stiff and Nonstiff Systems of Ordinary Differential Equations. *SIAM Journal on Scientific and Statistical Computing*, *4*. https://doi.org/10.1137/0904010

Pogoreutz, C., Rädecker, N., Cárdenas, A., Gärdes, A., Voolstra, C. R., & Wild, C. (2017). Sugar enrichment provides evidence for a role of nitrogen fixation in coral bleaching. *Global Change Biology*, *23*(9), 3838–3848. https://doi.org/10.1111/gcb.13695

Ponce-Alvarez, A., Mochol, G., Hermoso-Mendizabal, A., de la Rocha, J., & Deco, G. (2020). Cortical state transitions and stimulus response evolve along stiff and sloppy parameter dimensions, respectively. *ELife*, *9*. https://doi.org/10.7554/eLife.53268

Quinn, K. N., Abbott, M. C., Transtrum, M. K., Machta, B. B., & Sethna, J. P. (2023). Information geometry for multiparameter models: new perspectives on the origin of simplicity. *Reports on Progress in Physics*, *86*(3), 035901. https://doi.org/10.1088/1361-6633/aca6f8

Rabinovich, M. I., Varona, P., Selverston, A. I., & Abarbanel, H. D. I. (2006). Dynamical principles in neuroscience. *Reviews of Modern Physics*, *78*(4), 1213–1265. https://doi.org/10.1103/RevModPhys.78.1213

Rinaldi, S., & Scheffer, M. (2000). Geometric Analysis of Ecological Models with Slow and Fast Processes. *Ecosystems*, *3*(6), 507–521. https://doi.org/10.1007/s100210000045

Roach, D. R., Leung, C. Y., Henry, M., Morello, E., Singh, D., Di Santo, J. P., Weitz, J. S., & Debarbieux, L. (2017). Synergy between the Host Immune System and Bacteriophage Is Essential for Successful Phage Therapy against an Acute Respiratory Pathogen. *Cell Host Microbe*, *22*(1), 38-47.e4. https://doi.org/10.1016/j.chom.2017.06.018

Rocha, J. C., Peterson, G., Bodin, Ö., & Levin, S. (2018). Cascading regime shifts within and across scales. *Science*, *362*(6421), 1379–1383. https://doi.org/doi:10.1126/science.aat7850

Roughgarden, J. (2023). Holobiont Evolution: Population Theory for the Hologenome. *The American Naturalist*, *201*(6), 763–778. https://doi.org/10.1086/723782

Roughgarden, J. (2024). Lytic/Lysogenic Transition as a Life-History Switch. *Virus Evolution*, *10*(1). https://doi.org/10.1093/ve/veae028

Scheffer, M. (2009). *Critical Transitions in Nature and Society*. Princeton University Press. https://doi.org/10.2307/j.ctv173f1g1

Scheffer, M., Bascompte, J., Brock, W. A., Brovkin, V., Carpenter, S. R., Dakos, V., Held, H., van Nes, E. H., Rietkerk, M., & Sugihara, G. (2009). Early-warning signals for critical transitions. *Nature*, *461*(7260), 53–59. https://doi.org/10.1038/nature08227

Seekell, D. (2016). Passing the point of no return. *Science*, *354*(6316), 1109. https://doi.org/doi:10.1126/science.aal2188

Seekell, D. A., Carpenter, S. R., & Pace, M. L. (2011). Conditional Heteroscedasticity as a Leading Indicator of Ecological Regime Shifts. *The American Naturalist*, *178*(4), 442–451. https://doi.org/10.1086/661898

Shmulevich, I., & Kauffman, S. A. (2004). Activities and Sensitivities in Boolean Network Models. *Physical Review Letters*, *93*(4), 048701. https://doi.org/10.1103/PhysRevLett.93.048701

Silveira, C. B., Luque, A., Roach, T. N. F., Villela, H., Barno, A., Green, K., Reyes, B., Rubio-Portillo, E., Le, T., & Mead, S. (2019). Biophysical and physiological processes causing oxygen loss from coral reefs. *ELife*, *8*.

Silveira, C. B., Luque, A., & Rohwer, F. (2021). The landscape of lysogeny across microbial community density, diversity and energetics. *Environmental Microbiology*, *23*(8), 4098–4111. https://doi.org/10.1111/1462-2920.15640

So, J. W. H. (1979). A note on the global stability and bifurcation phenomenon of a lotka-volterra food chain. *Journal of Theoretical Biology*, *80*(2), 185–187. https://doi.org/10.1016/0022-5193(79)90204-2

Strogatz, S. H. (2001). Exploring complex networks. *Nature*, *410*(6825), 268–276. https://doi.org/10.1038/35065725

Strogatz, S. H. (2015). *Nonlinear dynamics and chaos : with applications to physics, biology, chemistry, and engineering*. Westview Press. https://search.library.wisc.edu/catalog/9910223127702121

Suttle, C. A., & Chen, F. (1992). Mechanisms and Rates of Decay of Marine Viruses in Seawater. *Applied and Environmental Microbiology*, *58*(11), 3721–3729. https://doi.org/10.1128/aem.58.11.3721-3729.1992

Swain, A., Hoffman, T., Leyba, K., & Fagan, W. F. (2021). Exploring the Evolution of Perception: An Agent-Based Approach. *Frontiers in Ecology and Evolution*, *9*. https://doi.org/10.3389/fevo.2021.698041

Thingstad, T. F. (2000). Elements of a theory for the mechanisms controlling abundance, diversity, and biogeochemical role of lytic bacterial viruses in aquatic systems. *Limnology and Oceanography*, *45*(6), 1320–1328. https://doi.org/10.4319/lo.2000.45.6.1320

Thingstad, T. F. (2022). Competition–defense trade-offs in the microbial world. *Proceedings of the National Academy of Sciences*, *119*(37). https://doi.org/10.1073/pnas.2213092119

Turchin, P. (2003). *Complex Population Dynamics: A Theoretical/Empirical Synthesis* (First Edition). Princeton University Press.

Våge, S., Storesund, J. E., & Thingstad, T. F. (2013). Adding a cost of resistance description extends the ability of virus–host model to explain observed patterns in structure and function of pelagic microbial communities. *Environmental Microbiology*, *15*(6), 1842–1852. https://doi.org/10.1111/1462-2920.12077

Varona, N. S., Hesketh-Best, P. J., Coutinho, F. H., Stiffler, A. K., Wallace, B. A., Garcia, S. L., Scholten, Y., Haas, A. F., Little, M., Vermeij, M., Luque, A., & Silveira, C. (2024). Host-specific viral predation network on coral reefs. *The ISME Journal*, *18*(1). https://doi.org/10.1093/ismejo/wrae240

Virtanen, P., Gommers, R., Oliphant, T. E., Haberland, M., Reddy, T., Cournapeau, D., Burovski, E., Peterson, P., Weckesser, W., Bright, J., van der Walt, S. J., Brett, M., Wilson, J., Millman, K. J., Mayorov, N., Nelson, A. R. J., Jones, E., Kern, R., Larson, E., … SciPy, C. (2020). SciPy 1.0: fundamental algorithms for scientific computing in Python. *Nature Methods*, *17*(3), 261–272. https://doi.org/10.1038/s41592-019-0686-2

Wadduwage, D. P., Wu, C. Q., & Annakkage, U. D. (2013). Power system transient stability analysis via the concept of Lyapunov Exponents. *Electric Power Systems Research*, *104*, 183–192. https://doi.org/10.1016/j.epsr.2013.06.011

Wang, R.-S., Saadatpour, A., & Albert, R. (2012). Boolean modeling in systems biology: an overview of methodology and applications. *Physical Biology*, *9*(5), 055001. https://doi.org/10.1088/1478-3975/9/5/055001

Weitz, J. S. (2016). *Quantitative Viral Ecology: Dynamics of Viruses and Their Microbial Hosts*. Princeton University Press.

Wigington, C. H., Sonderegger, D., Brussaard, C. P. D., Buchan, A., Finke, J. F., Fuhrman, J. A., Lennon, J. T., Middelboe, M., Suttle, C. A., Stock, C., Wilson, W. H., Wommack, K. E., Wilhelm, S. W., & Weitz, J. S. (2016). Re-examination of the relationship between marine virus and microbial cell abundances. *Nature Microbiology*, *1*, 15024.

Witt, M. C. (2019). *An analytical approach to transient dynamics: A case study on phage and bacteria population interactions* [Master]. San Diego State University.

Wolf, A., Swift, J. B., Swinney, H. L., & Vastano, J. A. (1985). Determining Lyapunov exponents from a time series. *Physica D: Nonlinear Phenomena*, *16*(3), 285–317. https://doi.org/10.1016/0167-2789(85)90011-9

Yuasa, A., Uehara, S., Ushizawa, K., Kodera, S., Arai, N., Hirata, A., & Otaka, Y. (2024). The thermal sensation threshold and its reliability induced by the exposure to 28 GHz millimeter-wave. *Frontiers in Neuroscience*, *18*. https://doi.org/10.3389/fnins.2024.1331416

Zhou, Y., Yu, H., Xu, S., Luo, M., & Zhou, X. (2022). High-density thermal sensitivity of the hand under different thermal states and stimulus intensities. *Indoor Air*, *32*(8). https://doi.org/10.1111/ina.13089

Zimring, J. C. (2019). *What science is and how it really works* (1st ed.). Cambridge University Press.